Journal Pre-proof

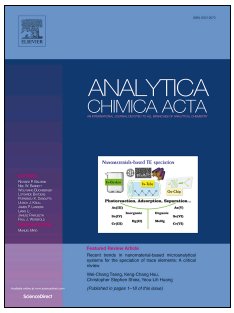

Assembling Reduced Graphene Oxide with Sulfur/Nitrogen- “Hooks” for Electrochemical Determination of Hg(II)

Cheng-Cheng Bi, Xu-Xu Ke, Xing Chen, Rohan Weerasooriya, Zhan-Yong Hong, Lian-Chao Wang, Yu-Cheng Wu

PII: S0003-2670(19)31425-4

DOI: https://doi.org/10.1016/j.aca.2019.11.062

Reference: ACA 237272

To appear in: *Analytica Chimica Acta*

Received Date: 25 October 2019

Revised Date: 13 November 2019

Accepted Date: 23 November 2019

Please cite this article as: C.-C. Bi, X.-X. Ke, X. Chen, R. Weerasooriya, Z.-Y. Hong, L.-C. Wang, Y.-C. Wu, Assembling Reduced Graphene Oxide with Sulfur/Nitrogen- “Hooks” for Electrochemical Determination of Hg(II), *Analytica Chimica Acta*, https://doi.org/10.1016/j.aca.2019.11.062.

Author Contributions:

Cheng-Cheng Bi：Methodology，Validation，Writing - Original Draft.

Xu-Xu Ke: Methodology，Validation.

Xing Chen: Conceptualization, Writing - Review & Editing, Supervision.

Rohan Weerasooriya: Writing- Reviewing and Editing.

Zhan-Yong Hong: Validation, Investigation.

Lian-Chao Wang: Methodology, Validation.

Yu-Cheng Wu：Funding acquisition.

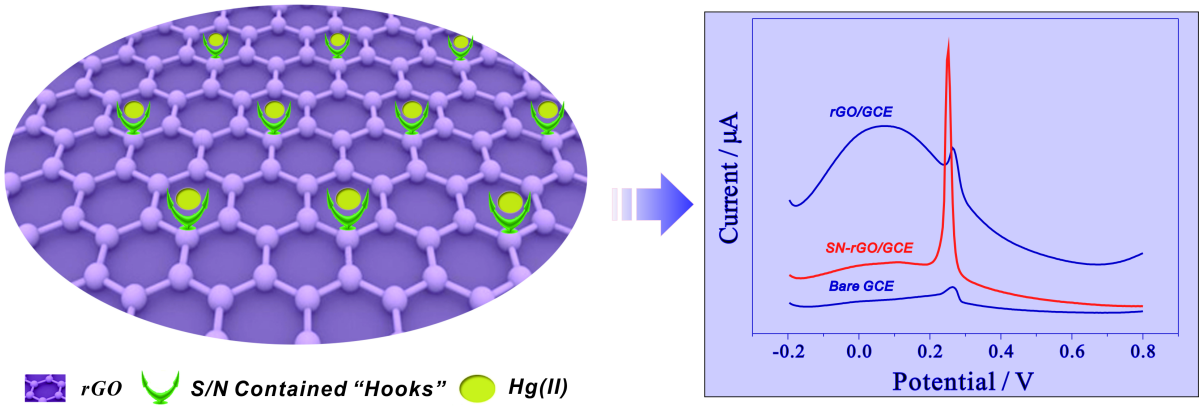

Assembling Reduced Graphene Oxide with Sulfur/Nitrogen- "Hooks" for Electrochemical Determination of Hg(II)

Cheng-Cheng Bi[a,b], Xu-Xu Ke [a,b], Xing Chen[*a,b,c], Rohan Weerasooriya[a,d], Zhan-Yong Hong[a], Lian-Chao Wang[*b], Yu-Cheng Wu[a,b]

[a] *Key Lab of Aerospace Structural Parts Forming Technology and Equipment of Anhui Province, Institute of Industry and Equipment Technology, Hefei University of Technology, Hefei, 230009, P. R. China*

[b] *School of Materials Science and Engineering, Hefei University of Technology, Hefei 230009, P. R. China*

[c] *School of Resources and Environmental Engineering, Hefei University of Technology, Hefei, 230009, P. R. China*

[d] *National Institute of Fundamental Studies，Kandy 20000，Sri Lanka*

Corresponding authors:

Xing Chen (xingchen@hfut.edu.cn);

Lian-Chao Wang (hfutwlc@163.com);

Abstract:

Herein the sulfur/nitrogen contained groups, serving as the "hooks" for electrochemical determination of Hg(II), were assembled on the reduced graphene oxide (hereafter SN-rGO) via a one-step facile hydrothermal method. The thiourea acts as a precursor for sulfur/nitrogen doping and partial reduction of graphene oxide. The SN-rGO was used to modify the glassy carbon electrode (GCE) for electrochemical detection of Hg(II) by square wave anodic stripping voltammetry (SWASV). The sulfur/nitrogen doping significantly improves the Hg(II) complexation by SN-rGO due to the creation of multifunctional groups on the graphene nanosheet. The SN-rGO modified electrode has excellent sensitivity (20.48 μA/μM) and limit of detection (LOD 8.93 nM) for Hg(II) detection. The newly developed Hg(II) sensing electrode possesses minimal interference for other ions typically found in natural waters. Therefore, it can be used for routine water quality monitoring. The fabrication of the SN-rGO electrode is rapid and low cost; hence, it offers a potential platform for environmental monitoring of toxic metal ions.

Key Words:

Reduced graphene oxide; Sulfur/nitrogen doping; Electrochemical detection; Mercury ions; Thiourea

1. Introduction

Mercury is a neurotoxic, carcinogenic, mutagenic, and teratogenic element that has complex chemistry in the environment [1]. Hg(II) is the most stable soft Lewis acid that can readily complex with S-containing ligands and undergoes methylation forming extremely toxic dimethylmercury complexes [2, 3]. To control global mercury emissions, 140 countries signed the Minamata Convention on Mercury [4]. Further, most of the mercury accumulated in fish and biota is stemmed from natural water. US EPA designates mercury as a primary contaminant with a maximum contaminant limit (MCL) is 2 μg/L in drinking water [5]. Therefore, the development of rapid and low-cost methods for trace detection of mercury species in water is a research priority.

To date, many analytical techniques are available for the detection of traces of mercury such as atomic absorption spectrometry[6], inductively coupled plasma mass spectrometry[7], X-ray fluorescence spectrometry [8], and enzyme-linked immunosorbent assay (ELISA) [9]. Although these methods are robust, reliable, and accurate, most of them are not suited for in situ detection of Hg(II). They are also costly and time-intensive that require skilled operations, which limit the applications in routine monitoring programs. On the contrary, the electroanalytical methods offer an attractive alternative due to their excellent sensitivity, selectivity, low capital cost, portability, and easy operations for metal ions detection in environmentally relevant concentrations[10-13] . In this context, the square wave anodic stripping voltammetry (SWASV) is particularly powerful for trace detection of mercury ions due to its high speed, enhanced sensitivity and inertness to dissolved gases as O_2[14]. Recently nanocomposite modified sensors have gained attention due to their excellent analytical performance and robustness in detecting heavy metal ions as Hg(II) under

SWASV mode [15, 16].

Graphene-based nanocomposite modified electrodes have widely been used for the detection of mercury ions at trace levels [17-21]. Zou et al.[17] used piperazine-grafted reduced graphene oxide modified glassy carbon electrode for efficient detection of Hg(II), which shows a wide linear range from 0.4-12 000 nM with a low detection of 0.2 nM. Gong et al.[18] reported monodispersed graphene decorated Au nanoparticles as an electrochemical sensor for ultra-sensitive stripping voltammetric detection of mercury ions. The Au-graphene nanocomposite facilitates efficient electron transfer which results in Hg (II) detection with high sensitivity, i.e., 708.3 μA/ppb with LOD as low as 6 ppt. Previously we prepared [19], nitrogen-doped reduced graphene oxide/MnO_2 nanocomposites for the detection of mercury ions. Nitrogen-doped graphene plays a dual role: it increases the relative density of active sites on the electrode surface; it also serves as a substrate for MnO_2 loading. The synergy between the two processes resulted in a highly selective substrate for mercuric ion detection with excellent sensitivity (72.16 μA/μM) and LOD (0.0414 nM). Zhao et al.[20] prepared nanocomposites containing polypyrrole and reduced graphene oxide for electrochemical detection of heavy metal ions based on the "selective adsorption toward toxic metal ions results in selective response" strategy. The introduction of active groups of nitrogen-containing elements into the composite greatly improved the electrochemical selectivity of mercury ions and excellent sensitivity (124 μA/μM), and limits of detection, LOD (15 nM) were obtained. Doping with foreign ions is effective to modify graphene with enhanced the performance for sensor applications.

It is also noted that hetero sulfur (S), nitrogen (N) functionalized nanomaterials have shown a high affinity to mercury ions [22-26]. Due to the high affinity of

mercury ions on N and S sites on 2,4,6-trimercaptotriazine (TMT), TMT incorporated Au nanocomposite modified electrodes were used for trace detection of metal ions[24]. Zhou et al.[27] reported a sensitive and selective electrochemical method for mercury ions detection by functionalizing graphene oxide with cysteine. The material selectively interacted with Hg(II) due to the presence of many -SH (mercapto) groups on graphene. Thiourea contains sulfur and nitrogen groups vital for the fabrication of new materials with a high affinity for metal ions. On several occasions, the thiourea-based new materials were used as an efficient adsorbent for the removal of mercury ions from the aqueous solutions [28, 29] and metal ions pre-concentration on the electrode surface as required in stripping electrochemical analysis [30, 31].

Based on the above enlightenment, we fabricated a nanocomposite via a one-step facile hydrothermal method for electrochemical Hg(II) detection, namely sulfur/nitrogen-doped reduced graphene oxide, utilizing graphene oxide and thiourea as starting materials. The sulfur/nitrogen contained groups serve as the “hooks” for Hg(II). The nanocomposite was extensively characterized by scanning/transmission electron microscopy, x-ray photon spectroscopy, Raman and Fourier transform infrared spectroscopic methods. The well-characterized nanocomposite was incorporated into a glassy carbon electrode electrochemical sensor for trace determination of mercury ions by SWASV. The performance of the modified GCE sensor was optimized to background electrolyte, pH, deposition potential, and time. The chemical interference from the matrix elements commonly found in natural waters for Hg (II) detection was also evaluated. The stability of the SN-rGO SCE for repeated used for Hg (II) detection was also examined. Finally, the newly developed GCE modified sensor was used for mercuric ions detection spiked in natural waters.

2. **Experimental**

2.1. Chemicals and reagents

All chemicals were analytical grade and used as received. 0.1 M acetate buffer solution (ABS) for different pH was prepared by mixing 0.1M NaAc and 0.1M HAc solutions in varying proportions. 0.1 M phosphate buffer solution (PBS) was prepared by mixing 0.1 M KH_2PO_4 and 0.1 M Na_2HPO_4 solutions. Sodium carbonate buffer solution (Na_2CO_3-$NaHCO_3$) of 0.1 M was prepared by mixing a stock solution of 0.1 M sodium carbonate and sodium bicarbonate. The water (18.2 MΩ cm) used was purified with the NANOpure Diamond UV water system.

2.2. Methods

All electrochemical measurements were carried out using a computer-controlled potentiostat (CHI 660D CHI Instruments Co., Shanghai, China). A conventional three-electrode configuration was used: working electrode – a bare or modified electrode, reference electrode - Ag/AgCl/$KCl_{saturated}$ electrode, and counter electrode - Pt wire. The morphology of the nanomaterials was investigated by field-emission scanning electron microscopy (SEM, Quanta 200 FEI Company, USA) and transmission electron microscopy (JEM-2100, Japan). Surface elemental composition and chemical oxidation states were determined by X-ray photoelectron spectroscopy (XPS) using an Mg Ka X-ray source (1253.6 eV, 120 W) at a constant analyzer (VG ESCALAB MKII, USA).

The structure of characteristic of the samples were analyzed using a Fourier transform infrared (FTIR) spectrometer (Nicolet 67, Thermo Nicolet Co., USA) in the specular transmission mode, the spectra were acquired in the range 500-4000 cm^{-1}, KBr was used after dryness under the infrared lamp, the mass proportion of sample material and KBr was 1:100, and the mixture was ground fully in a mortar. Raman

spectra were obtained with a laser excitation of Ar^+ laser at a wavelength of 532 nm (LabRAM HR800 HORIBA Jobin Yvon, FR).

2.3. Preparation of functionalized SN-rGO nanostructures

Graphene oxide was first synthesized by the modified Hummers' method [32]. The graphene-thiourea composite was synthesized by a hydrothermal method, as shown below. A 40 mg graphene oxide powder was well dispersed in 80 mL deionized water and ultrasonicated for 30 min. To examine the influence of different content of thiourea doped into the graphene on the electrochemical analysis of Hg(II), 1-4 mmol thiourea was added into the suspension and stirred well. The mixture was transferred into a Teflon-lined autoclave (100 mL capacity) and heated at 180℃ in an oven for 12 h and then cooled to ambient room temperature. The resultant black color material was washed with deionized water several times and dried at 60℃for 24 h. The sulfur/nitrogen-doped graphene samples with different contents of thiourea precursor are labeled as SN-rGO-x (x represents the amount of thiourea (mmol) added into the suspension, x=1, 2, 3, 4.). As a control, reduced graphene oxide (rGO) was prepared under the same conditions without adding thiourea. The glassy carbon electrodes modified with SN-rGO-x were used to determine maximum stripping current for 0.1 μM Hg (II). Out of the SN-rGO-x GCE electrodes used, SN-rGO-2 GCE showed maximum stripping current for Hg (II) (Shown in Figure S3). We used SN-rGO-2 (hereafter referred SN-rGO) for all subsequent studies.

2.4. Preparation of modified electrodes and measurement procedures

Before modification, the bare GCE with a diameter of 2 mm was sequentially polished with 1.0 μm, 0.3 μm and 0.05 μm alumina powder slurries to yield a shiny

surface, and then successively sonicated with 1:1 HNO_3 solution, ethanol and deionized water for 2 min to remove any contaminants from the electrode surface. The SN-rGO has dissolved in N, N-dimethyl formamide (DMF) and sonicated for 30 min to yield a homogeneous suspension. An appropriate amount of the suspension was pipetted onto the freshly polished GCE surface and dried under a nitrogen atmosphere. For a comparison, rGO modified GCE was also prepared. The surface of the modified electrode was regenerated by polishing before the next measurement.

The square wave anode stripping voltammetry (SWASV) method was used to analyze Hg(II) in 10 mL 0.1 M ABS pH 5.00 buffer. The Hg(II) deposition was carried out at -1.0 V applied potential for 150 s under stirring. The SWASV signal was recorded between -0.2 V and -0.8 V with 4 mV steps, 25 mV amplitude, and 15 Hz frequency without stirring. All experiments were carried out at ambient conditions.

2.5. Hg(II) adsorption measurements

Typically, 30 mg rGO and SN-rGO were mixed with 5 mL 100 μM Hg(II) in deionized water. These two mixed solutions were sonicated for 30 min. and waited for 5 h. The Hg(II) sorbed rGO and SN-rGO samples were washed several times with deionized water and vacuum dried overnight for XPS analysis.

3. Results and discussion

3.1. Characterization of rGO and SN-rGO

Figures 1 show transmission electron microscopy (TEM) images and EDX elemental distribution maps of rGO and SN-rGO. As shown in Figure 1 (a), the SN-rGO consists of smooth flat thin sheets with small wrinkles at the edges. The average composition of SN-rGO contains a C: O: S: N atomic ratio of 90.95: 7.22:

1.00: 0.83. The uniform pattern of C, O, S and N distribution maps confirm that sulfur- and nitrogen- groups are successfully functionalized onto rGO.

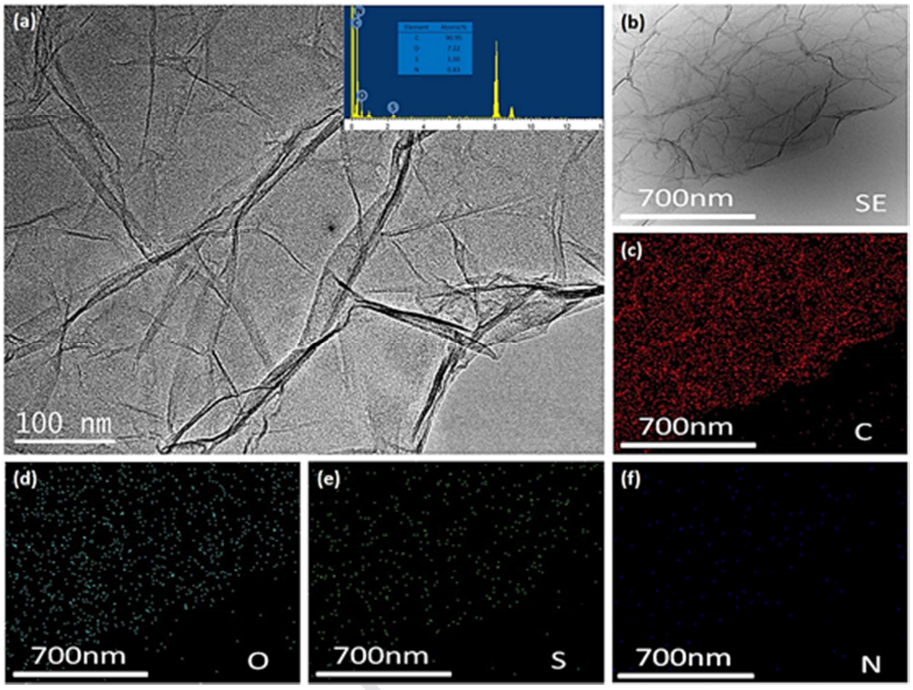

Figure 1. (a) TEM images of the synthesized SN-rGO, the inset is EDS analysis of SN-rGO. The EDS mapping of C (c), O (d), S (e), and N (f). Selected area for elemental mapping (b).

The rGO and SN-rGO samples were also characterized by Raman spectroscopy, infrared spectroscopy (FTIR) and x-ray photon spectroscopy (XPS). Figure 2(a) shows a representative Raman spectrum of rGO and SN-rGO used. The characteristic broad D (1352 cm^{-1}) and G bands (1593 cm^{-1}) are present in both samples. The degree of graphene disorder depends on the D and G bands intensity ratio, i.e. $\left(\frac{I_D}{I_G}\right)$. The $\left(\frac{I_D}{I_G}\right)$ ratios for rGO and SN-rGO were 1.01 and 1.11, respectively. Thiourea treatment on graphene i.e. SN-rGO shows higher defects density when compared to rGO. Figure 2. (b) shows the infrared spectra of GO, rGO, and SN-rGO samples. In all samples, the band at 3409 cm^{-1} is ascribed to stretching vibrations of hydroxyl groups. The

band at 1620 cm^{-1} is due to skeletal vibrations of un-oxidized graphitic domains. The C=O deformations of -COOH are shown at 1734 cm^{-1}. The bands at 1382 and 1070 cm^{-1} correspond to C-O-H deformation and C-O stretching vibrations, respectively. The spectrum of rGO retains bands at O-H (3425 cm^{-1}), C=O (1710 cm^{-1}) and C=C (1580 cm-1) which indicates GO→ rGO partial reduction. Thiourea is a strong reductant for GO [33]. Therefore when compared to GO, the band intensities of SN-rGO at 3410 (O-H) and 1100 (C-O) cm^{-1} in SN-rGO have decreased dramatically [33]. Besides, in SN-rGO the bands at 1698 cm^{-1} and 1640 cm^{-1} confirm the presence of –CO-S and –CO-N- groups [34]. Therefore, infrared data confirm chemically grafted sulfur- and nitrogen- groups on rGO.

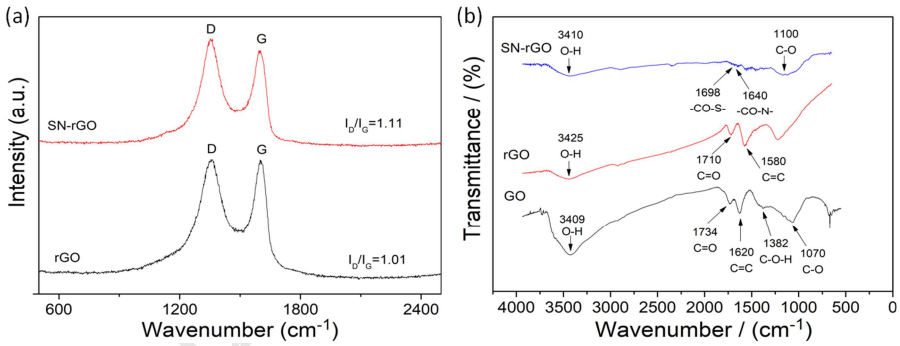

Figure 2. (a)Raman spectra of rGO and SN-rGO, (b)FTIR spectra of GO, rGO and SN-rGO.

To further confirm the chemical nature of the new materials, X-ray photoelectron spectroscopy (XPS) analysis was performed. The survey scan of SN-rGO (Figure 3a) shows the identical elemental composition with EDS data. The S and N contents were 2.01 and 1.71 atom%, respectively, which indicates that a relatively large amount of S and N atoms was doped into SN-rGO. The high-resolution XPS spectrum of C1s in SN-rGO (Figure 3b) can be de-convoluted into several single peaks: C-C(284.75 eV), C-OH(285.32 eV), C=O(286.18 eV), COOH(287.85 eV), C-S-C (283.90 eV) [35] and C-N-C (286.59 eV) [36], which further confirm that S and N are doped into the

graphene sheets. All of the high-resolution S 2p peaks of SN-rGO were fitted to three components centered at approximately 164, 165, and 168eV, respectively (Figure 3.c). The former two peaks correspond to S $2p_{3/2}$(S-1) and S $2p_{1/2}$(S-3) positions derived from spin−orbit splitting of thiophenic sulfur atoms incorporated into the carbon framework. The last peak (S-2) indicates oxidation of sulfur[37]. On the other hand, in high-resolution XPS spectra, N 1s also resolved into three peaks centered at 398.79, 400.03 and 401.10 eV correspond to pyridinic nitrogen (N-2), pyrrolic nitrogen (N-1) and graphitic nitrogen (N-3), respectively [38].

The C 1s core XPS spectrum of GO nanosheets (Figure S1b) can be resolved into five peaks with binding energies (BEs) at about 283.93, 284.86, 286.80, 287.23, and 288.61 eV due to sp^2-hybridized carbon, sp^3-hybridized carbon, C-O, C=O, and O-C=O species, respectively [39]. For rGO (Figure S2b), the oxygen-containing groups (COOH, C=O, and C-OH) decreased upon the reduction of graphene oxide.

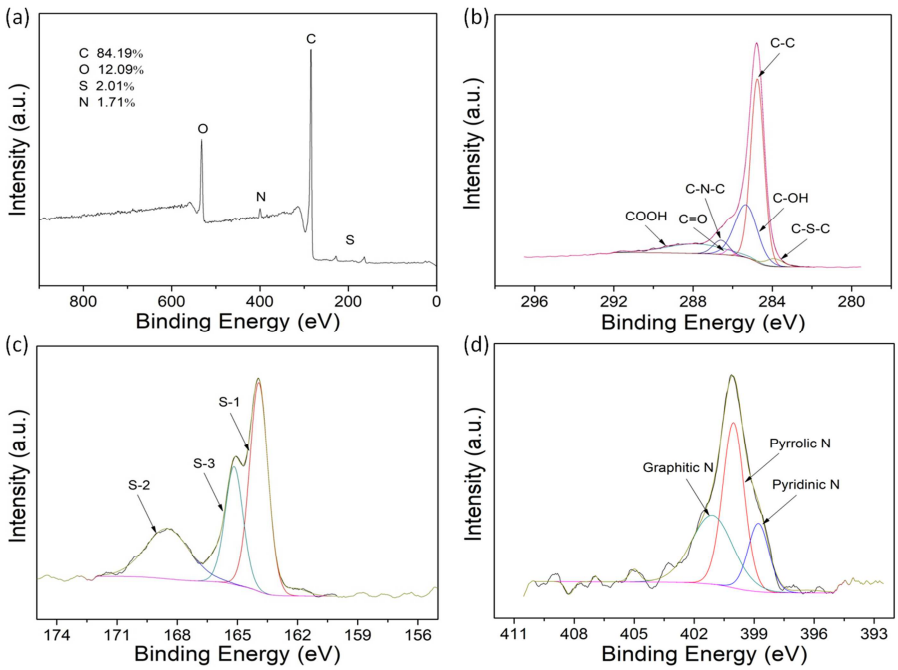

Figure 3. XPS spectra (a) high-resolution C1s spectra (b), S2p(c), and N1s (d) of SN-rGO.

3.2. Electrochemical characterization of SN-rGO

Cyclic voltammetry (CV) and electrochemical spectroscopy (EIS) were used to characterize the electrochemical performance of SN-rGO modified GCE (hereafter SN-rGO GCE), which can show explicit information about electron transfer kinetics of the redox couples. The SN-rGO GCE characterization was performed in 5 mM $Fe(CN_6)^{3-/4-}$ and 0.1 M KCl solutions. As shown in Figure 4(a) the anode and cathode currents peaks of the SN-rGO modified electrode are higher than that of rGO.

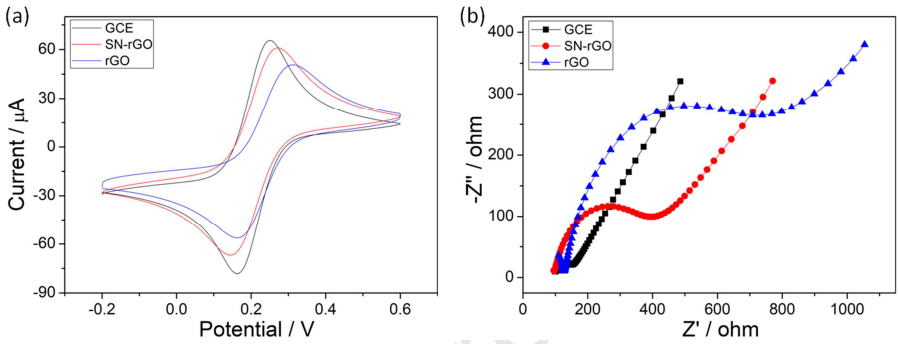

Figure 4. The CV (a) and EIS (b) measured with bare, rGO and SN-rGO nanomaterial modified GCE in the solution of 5mM $Fe(CN_6)^{3-/4-}$ containing 0.1M KCl.

EIS data are used to resolve the interfacial processes of rGO and SN-rGO modified electrodes. As in Figure 4b, a semi-circle and a linear portion in a typical Nyquist plot correspond to the electron transfer resistance (R_{et}) and diffusion-limited processes respectively. The equivalent electrical circuit was used to fit the EIS data (Figure S5). As in Figure 4 (b), for bare GCE small semi-circle implies a low electron transfer resistance of the redox couple (Table S1, the R_{et} of GCE ~95.56Ω). When the GCE is modified with SN-rGO or rGO, the corresponding R_{et} values are 354.3 Ω and 796.1Ω, respectively. We used a hydrothermal method to fabricate rGO. Therefore, the degree of GO reduction is not high, which results in an increase of R_{et} in rGO. In SN-rGO, the oxygen-containing functional groups decreased with commitment reduction of R_{et} value. In all cases, the CV and EIS diagrams of rGO ad SN-rGO

matched perfectly.

Bare GCE, rGO, and SN-rGO GCE were chosen to determine the efficacy of electrodes to determine Hg(II) under SWASV mode. As shown in Figure 5 (a), the stripping currents of 1.0μM Hg(II) in 0.1M acetate buffer (pH=5.0) were estimated using bare, rGO, and SN-rGO GCE electrodes. The stripping current at three types of electrodes varies in order: bare GCE < rGO < SN-RGO. Therefore, SN-rGO GCE shows excellent electrochemical performance for Hg(II) detection when compared to rGO or bare GCE. As discussed in an earlier section, the SN-rGO contains a high proportion of S- and N- groups that readily chelate Hg(II) enhancing electrochemical performance.

3.3. Optimization of Hg(II) detection

To estimate the best experimental parameters for Hg(II) detection, SN-rGO modified GCE was used by SWASV to optimize to following parameters: supporting electrolyte, solution pH, deposition potential and time. The efficiency of stripping responses of SN-rGO/GCE for 1.0 μM Hg(II) was examined using three electrolytes: viz. 0.1 M NaAc-HAc, PBS, and Na_2CO_3-$NaHCO_3$ buffer solutions. Always the system pH was at 5.0. The depositional potential and time were set at -1.0 V and 150 s, respectively. When compared to PBS or Na_2CO_3-$NaHCO_3$ buffers, 1.0 μM Hg(II) in 0.1 M NaAc-HAc shows the highest stripping current. Therefore, the 0.1M NaAc-HAc buffer system was used for further analysis.

The effect of stripping current for Hg(II) detection was examined as a function of solution pH. A series of 1.0 μM Hg(II) solutions were prepared in 0.1 M NaAc-HAc at pre-defined pH values. Pre-defined pH values of the buffer solutions were achieved by mixing 0.1 M NaAc and 0.1M HAc in different proportions. The stripping current

for 1.0 μM Hg(II) in NaAc-HAc was measured with SN-RGO modified GCE sensor. For this particular system, the stripping current is optimal between pH 4.0 and 6.0. Our data are in agreement with published data where Hg(II) detection was carried out with N-rGO /MnO_2 modified GCE [40]. When pH > 6, Hg(II) tends to hydrolyze, thus reduces the sensitivity of the GCE; when pH < 4, surface destruction of the electrode is noted. Around pH 5.0 Hg(II) stripping current is optimal detection for SN-rGO modified GCE sensor.

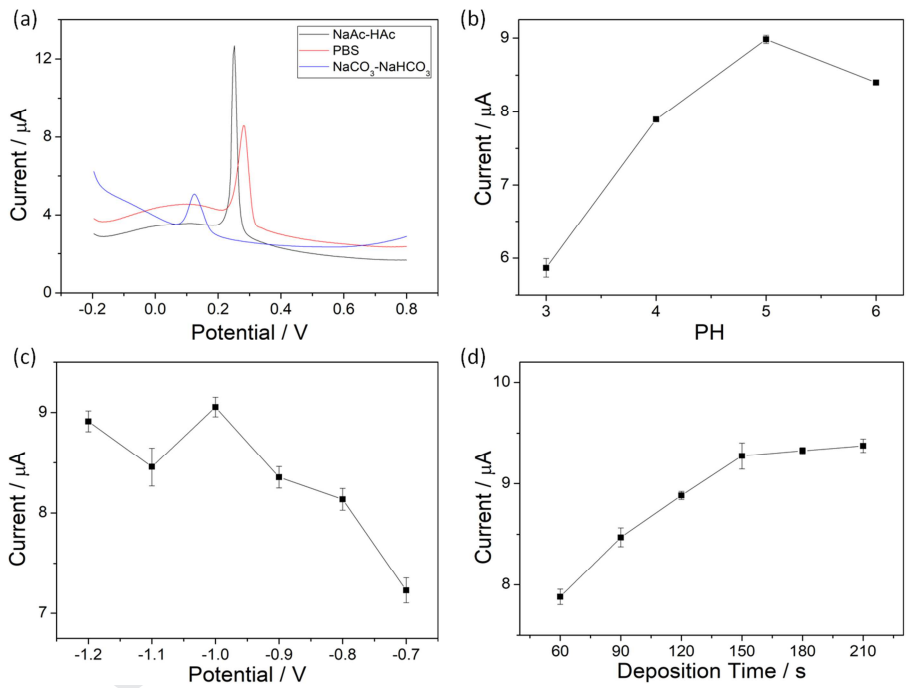

Figure 5. Optimization of experimental parameters for Hg (II) detection. Variation of (a) applied potential vs. stripping current measured in the different supporting electrolyte; (b) pH vs. striping current measured in 0.1M NaAc-HAc; (c) deposition potential with stripping current in 0.1M NaAc-HAc at pH 5.0; and (d) deposition time vs. stripping current in 0.1M HAc-NaAC at pH 5.0. on the electrochemical responses of the SN-rGO nanomaterial modified GCE was used by SWASV using 1.0μM Hg(II).

Optimal deposition potential for the SN-rGO GCE system was examined in 1.0 μM Hg(II) at pH=5 in NaAc-HAc buffer solutions. The potential at the modified GCE was changed between -1.2 and -0.7 V, and the results are shown in Figure 5c. When

the deposition potential shifts from -1.0 to -0.7 V, the stripping current reduced markedly due to the low adsorption of Hg(II). At extremely negative potentials, the evolution of H_2 is observed [40]. The H_2 poisons the electrode surface materials, which may hinder Hg(II) reduction. The optimal Hg(II) deposition potential of -1.0 V was chosen.

The optimal deposition time on modified GCE was examined in 1.0 μM Hg(II) at pH 5 with 0.1 M NaAC-HAc. The deposition time varied between 60 and 210 s. As shown in Figure 5 (d) the stripping current raises linearly with the extent of deposition time, reaching a plateau around 150 s. The 150 s deposition time was chosen. According to the data so far presented, the following optimal experimental conditions were used: pH 5 0.1 M NaAc-HAc, deposition time 150 s, and deposition potential -1.0 V.

3.4. **Electrochemical detection of Hg(II) with SN-rGO/GCE.**

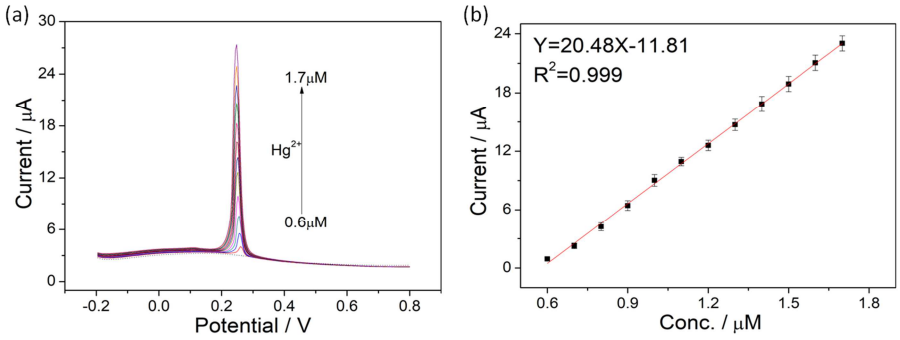

Figure 6. SWASV response (a) and the corresponding calibration plot (b) of the SN-rGO modified GCE toward Hg(II)

A Hg(II) detection method was developed with SN-rGO modified GCE electrode using SWASV in the 0.6-1.7μM concentration range. The resultant calibration curve plotted with current (μA) vs. Hg(II) concentration is shown in Figure 6, which shows a high correlation coefficient of 0.999. The calculated limit of detection (LOD) of

Hg(II) was 8.93 nM at a signal to noise ratio 3 (3δ method). Table S2 shows a summary of data reported for Hg(II) detection with other modified electrode–buffer systems. The SN-rGO modified GCE offers better results when compared to other methods. The sensitivity and the LOD values of our SN-rGO system are 20.48μA/μM and 8.93nM for Hg(II) detection under SWASV mode.

3.5. Possible mechanism of adsorption towards Hg(II)

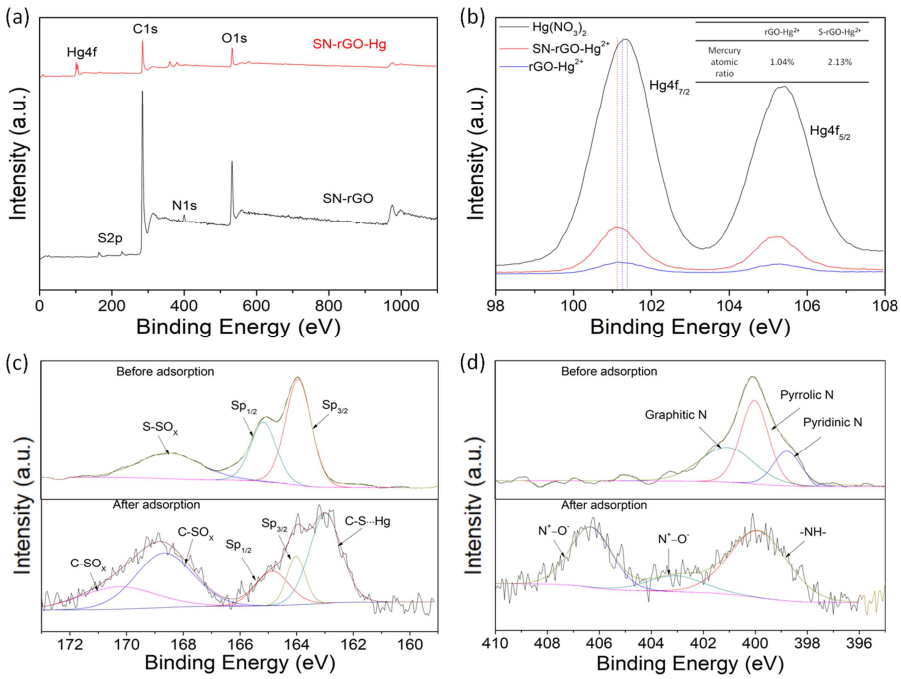

Figure 7. (a) XPS survey of SN-rGO before adsorption and after adsorption. (b)The comparison of SN-rGO and rGO in the adsorption of Hg(II). The inset is the mercury atomic ratio of rGO-Hg(II) and SN-rGO-Hg(II)

The mode of Hg(II) retention on the SN-rGO GCE surface was examined by XPS. The XPS spectrums of SN-rGO (black curve) and SN-rGO – Hg(II) (red curve) are shown in Figure 7(a). The appearance of a characteristic band at Hg4f confirms the presence of mercury on the SN-rGO surface. The relative affinity of Hg(II) on rGO and SN-rGO was also examined (Figure 7(b)). The intensity of the Hg $4f_{1/2}$ peak

in SN-rGO is higher than the rGO signal, which implies a strong affinity of Hg(II) on SN-rGO sites. Both in SN-rGO and rGO the Hg 4f peaks at 101.10 and 105.20 eV, 101.20 and 105.30 eV are observed. However, in pure $Hg(NO_3)_2$ only the peaks at 101.30 and 105.40eV are shown. When compared to rGO, in SN-rGO, the peak at 101.20 eV shifts into a negative direction by 0.1 eV, which indicates chemical interactions of Hg(II) with SN-rGO sites producing strong electrochemical signals on SN-rGO GCE. The Hg atomic composition on SN-rGO (2.13 %) is higher than rGO (1.04%) which indicates enhanced electrochemical activity on SN-rGO GCE (Figure S3 for details).

The high-resolution S 2p and N 1s spectra of the SN-rGO sample before and after Hg(II) adsorption were also measured. In Figure 7(c), S 2p could be classified into three major peaks before Hg(II) adsorption, and the de-convoluted peaks of the S 2p spectrum at 164.02 and 164.86 eV after adsorption can be assigned to S $p_{3/2}$ and S $p_{1/2}$ of thiophene sulfur, respectively, and peaks at 168.67 and 170.28 eV are related with S 2p electrons in C-SO_X groups, respectively. The new peak at 162.99 eV after the adsorption of Hg(II) could be assigned to Hg $4f_{7/2}$ electron in C-S···Hg[41]. Figure 7(d) shows the high-resolution XPS N 1s spectrum of the sample after Hg(II) adsorption, and N 1s is resolved into three peaks at 399.89, 403.06 and 406.33 eV. The peak at 399.89 V corresponding to –NH–; the peaks at 403.06 and 406.33 V related with N^+–O^-. The N 1s peaks change significantly upon Hg(II) adsorption, which demonstrates that the adsorption occurred on –NH– derived sites, which implied N-Hg multiple bond formation [42]. Our data show that Hg(II) has strong chemical interactions with the sulfur and nitrogen derived sites on SN-rGO, which shows “hooking” effects.

3.6. Chemical Interference with other cations

The interfering effect of Cd^{2+}, $Pb^{2+,}$ and Cu^{2+} on Hg(II) by SN-rGO modified GCE sensor was examined. The concentration of Hg(II) and interfering metal ions was kept at a 1:2 ratio either in single or multiple additions of foreign metal ions (hereafter single element mode and multiple elements mode respectively). As in Figure 8, in single element mode experiments, the effect of Cd^{2+} on the Hg(II) signal is not significant; Cu^{2+} reduces the Hg(II) to some extent. However, in the presence of Pb^{2+} in solution, the Hg(II) peak increased significantly, which is ascribed to the mutual promotion of adsorbed metal ions at the saturation. The behavior of Cd^{2+}, $Cu^{2+,}$ and Pb^{2+} with the Hg(II) is different. Conversely, in the relative intensities of Cd^{2+}, $Cu^{2+}$and Pb^{2+} increased in the presence of Hg(II), due to the formation of thin Hg film on the electrode surface. To enhance the detection limits of heavy metal ions, Hg film or Hg-based electrodes are used widely in electrochemical trace analysis. However, the methods based on Hg often impart a serious environmental concern [43-46]. The effect of Hg(II) signal in the simultaneous presence of other ions are shown in Figure 8(d). When compared to single element mode data, the Hg(II) signal decreased to some extent in multi-elements mode experiments due to possible formation of Hg amalgams, and the mutual competition of metal ions with Hg(II) for limited active sites on the modified electrode surface. However, the Hg(II) peak shape, sensitivity, and selectivity remain excellent regardless of the interfering heavy metal ions (The linear fitting data are shown in Figure S4).

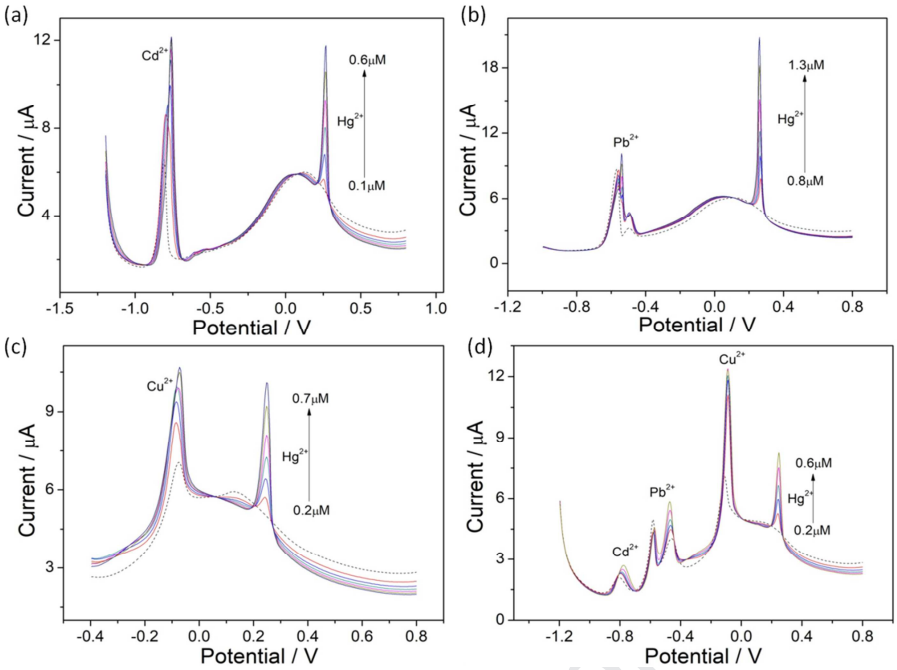

Figure 8. SWASV responses of the SN-rGO/GCE towards Hg(II) over a series of concentration range when adding (a) 0.5μM Cd^{2+}, (b) 0.5μM Pb^{2+}, (c) 0.5μM Cu^{2+}, and (d)0.5μM Cd^{2+}, Pb^{2+}, Cu^{2+}, simultaneously.

Additionally, bismuth ion (Bi^{3+}) was used for interference tests with similar electrochemical characteristics to Hg(II). It can be found that SN-rGO/GCE still has good sensitivity (20.48μA/μM) when a certain amount of Bi^{3+} was added (shown in Figure S5). This demonstrates that the SN-rGO modified GCE possesses excellent anti-interference performance, which might be attributed to the complexation between Hg(II) and sulfur/nitrogen active sites.

3.7. Stability and reproducibility

The stability of SN-rGO modified GCE was examined under the optimized conditions. Here, detection of 1.0 μM Hg(II) was carried out in twelve cycles using the same SN-rGO GCE. From Figure 9a, there are no obvious changes in stripping currents during repeated measurements (relative standard deviation (RSD) 2.16%). In

addition, the reproducibility measurements were carried out for 1.0μM Hg(II) using six SN-rGO electrodes (No. E1-E6), and the SWASV response was shown in Figure 9b RSD 3.25%, was lower than 5%, which indicates excellent reproducibility. The SN-rGO/GCE exerts superb stability and reproducibility, which has a potential for application of Hg(II) detection in environmental analysis.

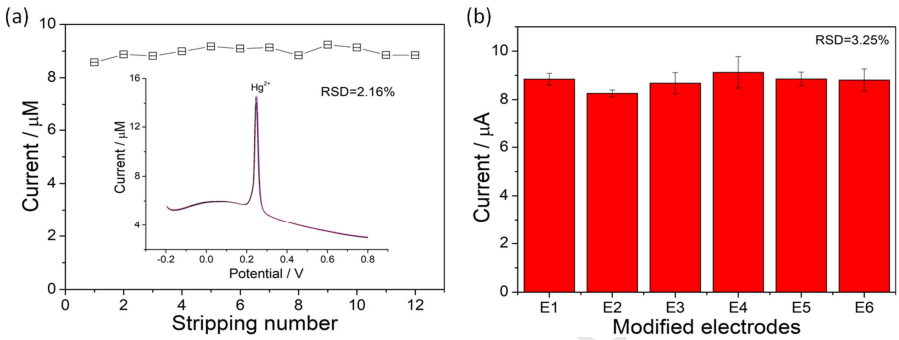

Figure 9. Stability and reproducibility of Hg(II) by SN-rGO GCE (a) SWASV responses of the SN-rGO/GCE to 1.0 μM Hg(II) during twelve successive cycles. (b) SWASV responses to-1.0 μM Hg(II) measured with six SN-rGO GCE

3.8. Real sample analysis

To assess the validity of our SN-rGO GCE sensor, Hg(II) detection was carried out using natural lake water samples collected from Hubing Tang water in Hefei University of Technology, Hefei City, Anhui Province, China. The water sample was buffered to pH 5.0 with 0.1M NaAc-HAc. Direct scanning of the lake water sample found no detectable Hg(II) species. Spiked Hg(II) concentrations were from 0.6μM to 1.0μM (Shown in Figure S6). Recovery experiments were carried out spiking Hg(II) into the lake water. As in Table 1, the spike recoveries of Hg(II) are excellent, i.e., 96.7 – 102.7 %. The relative standard deviation (RSD) of the results are in between 0.836 to 1.813 %. The results indicate minimal interference from the matrix in natural water for the Hg(II) detection, and the SN-rGO modified GCE sensor can be used for Hg(II) detection in natural water samples with minimal sample preparations.

Table 1. Determination of spiked Hg(II) in the lake water sample using the SN-rGO modified GCE (n=3).

Sample	Concentration		Recovery (%)	RSD (%)
	Added (μM)	Detected (μM)		
Lake water	0.6	0.61595±0.00515	102.7	0.836
	0.7	0.69350±0.01170	99.1	1.687
	0.8	0.77345±0.01385	96.7	1.791
	0.9	0.87405±0.01585	97.1	1.813
	1.0	0.99435±0.01385	99.4	1.392

4. Conclusions

We used thiourea to enhance the metals "hooking" ability of reduced graphene by one facile hydrothermal method. Our SN-rGO GCE shows excellent properties for trace detection of Hg(II) ions with a sensitivity (20.48μA/μM) and a limit of detection (8.93nM). The stability and data reproducibility of the S-rGO GCE for Hg(II) at repeated cycles is high. Our S-rGO GCE electrode is used in the trace detection of Hg(II) in natural water samples. Extension of the proposed method for multi-element detection protocols is in progress. The new electrochemical sensor technology holds a great promise for in situ trace detections of metal ions in the water.

Acknowledgments

The authors acknowledge the financial support from National Natural Science

Foundation of China (Grant No. 21777164)，National Basic Research Program of China (Grant No. SQ2019YFC040023)，Fundamental Research Funds for the Central Universities (Grant No. PA2019GDQT0019, and PA2019GDQT0017), and Key Technologies R & D Program of Anhui Province (No. 1704c0402195). R. W. acknowledges the Program of Distinguished Professor in B&R Countries (Grant No. DL20180052).

References:

[1] M. Gochfeld, Ecotoxicology and Environmental Safety, 56 (2003) 174.

[2] J. Aaseth, B. Hilt, G. Bjørklund, Environmental Research, 164 (2018) 65.

[3] G. Bjørklund, M. Dadar, J. Mutter, J. Aaseth, Environmental Research, 159 (2017) 545.

[4] Y. Lin, S.X. Wang, Q.R. Wu, T. Larssen, Environ Sci Technol, 50 (2016) 2337.

[5] U. EPA, (2019).

[6] R.F. Bendl, J.T. Madden, A.L. Regan, N. Fitzgerald, Talanta, 68 (2006) 1366.

[7] C.-H. Yao, S.-J. Jiang, A.C. Sahayam, Y.-L. Huang, Microchemical Journal, 133 (2017) 556.

[8] T. Swanston, T. Varney, I. Coulthard, G.N. George, I.J. Pickering, R. Murphy, D.M.L. Cooper, Journal of Archaeological Science, 58 (2015) 26.

[9] H. He, F. Wu, M. Xu, S. Yang, C. Sun, Y. Yang, Analytical Methods, 3 (2011) 1859.

[10] M. Zaib, M.M. Athar, A. Saeed, U. Farooq, Biosensors and Bioelectronics, 74 (2015) 895.

[11] D. Martín-Yerga, M.B. González-García, A. Costa-García, Talanta, 116 (2013) 1091.

[12] H.Q. Huang, L. Chen, S.Q. Wang, P. Kang, X.X. Chen, Z. Guo, X.J. Huang, Trac-Trend Anal Chem, 119 (2019).

[13] Y.X. Li, M. Yang, P.H. Li, S.H. Chen, Y.Y. Li, Z. Guo, S.S. Li, M. Jiang, C.H. Lin, X.J. Huang, Small (2019).

[14] D. Jadreško, M. Lovrić, Electrochimica Acta, 53 (2008) 8045.

[15] S. Yuan, D. Peng, D. Song, J. Gong, Sensors and Actuators B: Chemical, 181 (2013) 432.

[16] N. Zhou, J. Li, H. Chen, C. Liao, L. Chen, Analyst, 138 (2013) 1091.

[17] Y.X. Zuo, J.K. Xu, H.K. Xing, X.M. Duan, L.M. Lu, G. Ye, H.Y. Jia, Y.F. Yu, Nanotechnology, 29 (2018).

[18] J. Gong, T. Zhou, D. Song, L. Zhang, Sensors and Actuators B: Chemical, 150 (2010) 491.

[19] G.-L. Wen, W. Zhao, X. Chen, J.-Q. Liu, Y. Wang, Y. Zhang, Z.-J. Huang, Y.-C. Wu, Electrochimica Acta, 291 (2018) 95.

[20] Z.-Q. Zhao, X. Chen, Q. Yang, J.-H. Liu, X.-J. Huang, Chemical Communications, 48 (2012) 2180.

[21] A.R. Thiruppathi, B. Sidhureddy, W. Keeler, A.C. Chen, Electrochem Commun, 76 (2017) 42.

[22] V. Somerset, J. Leaner, R. Mason, E. Iwuoha, A. Morrin, Electrochimica Acta, 55 (2010) 4240.

[23] F.S. Awad, K.M. AbouZeid, W.M. Abou El-Maaty, A.M. El-Wakil, M.S. El Shall, Acs Appl Mater Inter, 9 (2017) 34230.

[24] J. Jayadevimanoranjitham, S.S. Narayanan, Applied Surface Science, 448 (2018) 444.

[25] P.L. Yap, S. Kabiri, D.N.H. Tran, D. Losic, Acs Appl Mater Inter, 11 (2019) 6350.

[26] T. V., K. P., Journal of Environmental Chemical Engineering, 7 (2019) 21.

[27] H. Zhou, X. Wang, P. Yu, X. Chen, L. Mao, Analyst, 137 (2012) 305.

[28] O. Olkhovyk, V. Antochshuk, M. Jaroniec, Colloids and Surfaces A: Physicochemical and Engineering Aspects, 236 (2004) 69.

[29] M. Mureseanu, A. Reiss, N. Cioatera, I. Trandafir, V. Hulea, Journal of Hazardous Materials, 182 (2010) 197.

[30] A. Walcarius, C. Delacôte, Analytica Chimica Acta, 547 (2005) 3.

[31] W. Deng, Y. Tan, Y. Li, Y. Wen, Z. Su, Z. Huang, S. Huang, Y. Meng, Q. Xie, Y. Luo, S. Yao, Microchimica Acta, 169 (2010) 367.

[32] W.S. Hummers, R.E. Offeman, Journal of the American Chemical Society, 80 (1958) 1339.

[33] Y. Liu, Y. Li, Y. Yang, Y. Wen, M. Wang, Journal of Nanoscience and Nanotechnology, 11 (2011) 10082.

[34] W.S.V. Lee, M. Leng, M. Li, X.L. Huang, J.M. Xue, Nano Energy, 12 (2015) 250.

[35] S. Wan, L. Wang, Q. Xue, Electrochemistry Communications, 12 (2010) 61.

[36] Y. Zheng, Y. Jiao, J. Chen, J. Liu, J. Liang, A. Du, W. Zhang, Z. Zhu, S.C. Smith, M. Jaroniec, G.Q. Lu, S.Z. Qiao, Journal of the American Chemical Society, 133 (2011) 20116.

[37] S. Yang, L. Zhi, K. Tang, X. Feng, J. Maier, K. Müllen, Advanced Functional Materials, 22 (2012) 3634.

[38] Y. Wang, Y. Shao, D.W. Matson, J. Li, Y. Lin, ACS Nano, 4 (2010) 1790.

[39] D. Long, W. Li, L. Ling, J. Miyawaki, I. Mochida, S.-H. Yoon, Langmuir, 26 (2010) 16096.

[40] A. Królicka, A. Bobrowski, A. Kowal, Electroanalysis, 18 (2006) 1649.

[41] F.S. Awad, K.M. AbouZeid, W.M.A. El-Maaty, A.M. El-Wakil, M.S. El-Shall, ACS Applied Materials & Interfaces, 9 (2017) 34230.

[42] H. Cui, Y. Qian, Q. Li, Q. Zhang, J. Zhai, Chemical Engineering Journal, 211-212 (2012) 216.

[43] H.P. Wu, Analytical Chemistry, 68 (1996) 1639.

[44] C. Agra-Gutiérrez, J.C. Ball, R.G. Compton, The Journal of Physical Chemistry B, 102 (1998) 7028.

[45] T.M. Florence, Journal of Electroanalytical Chemistry and Interfacial

Electrochemistry, 27 (1970) 273.

[46] R. Ouyang, Z. Zhu, C.E. Tatum, J.Q. Chambers, Z.-L. Xue, Journal of Electroanalytical Chemistry, 656 (2011) 78.

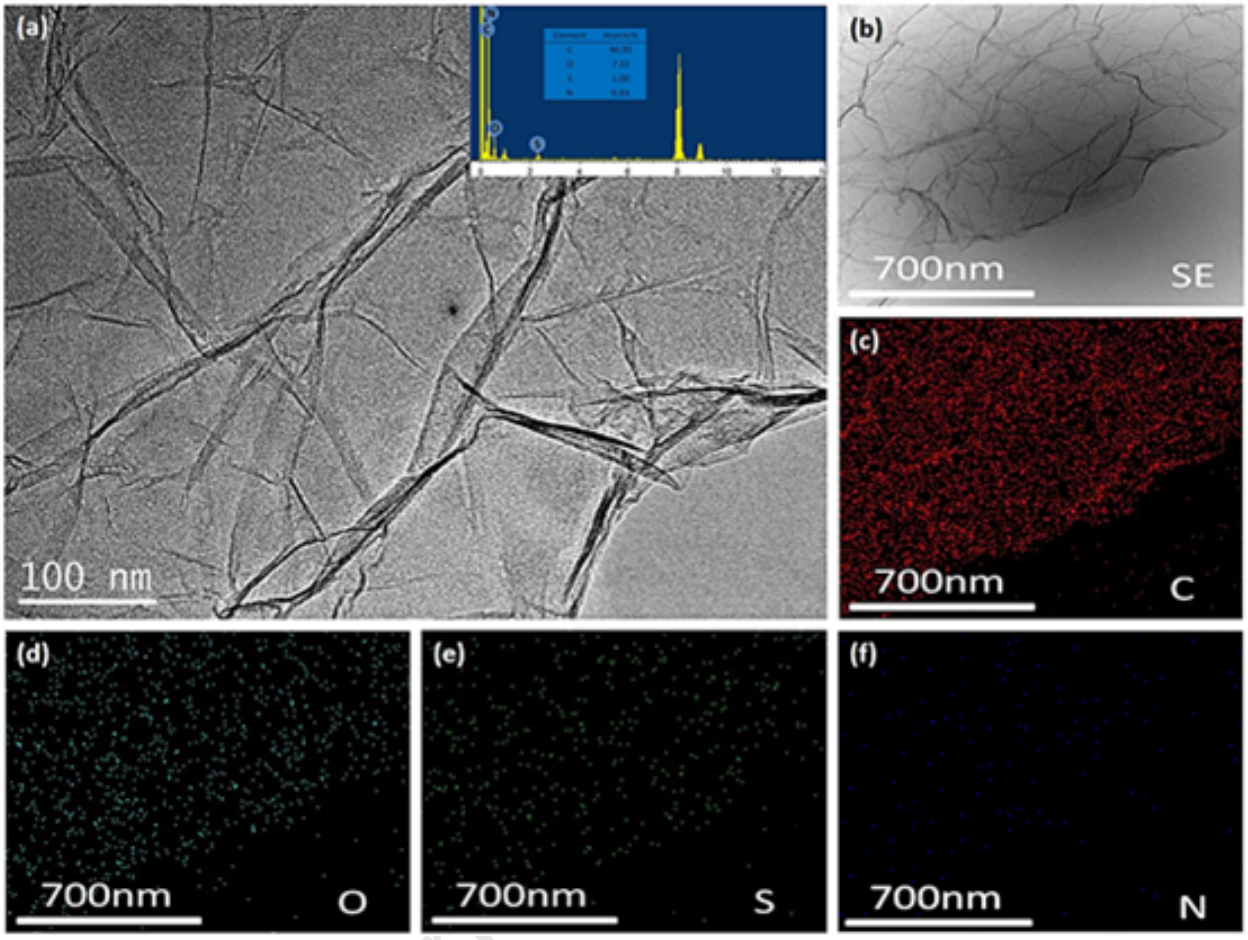

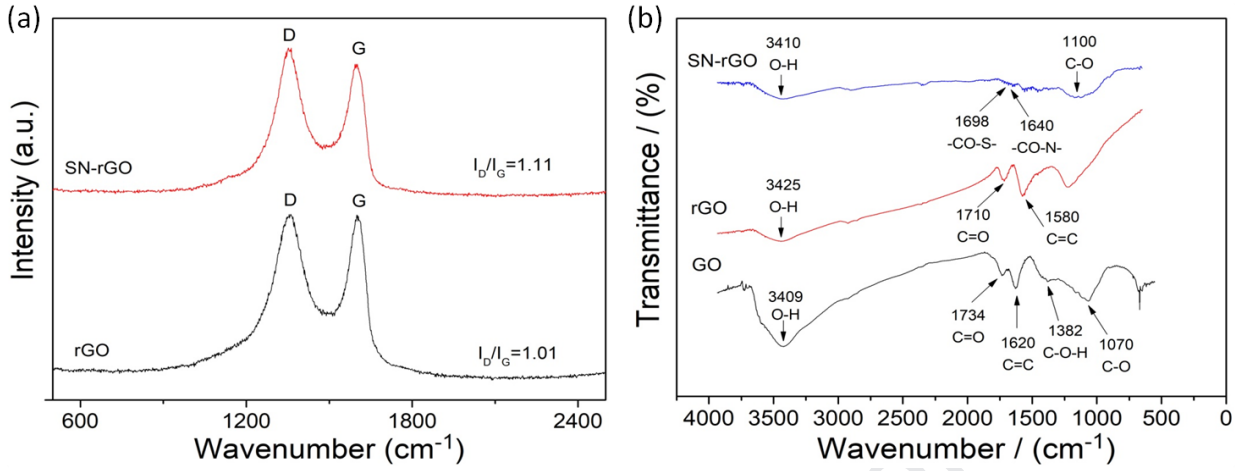

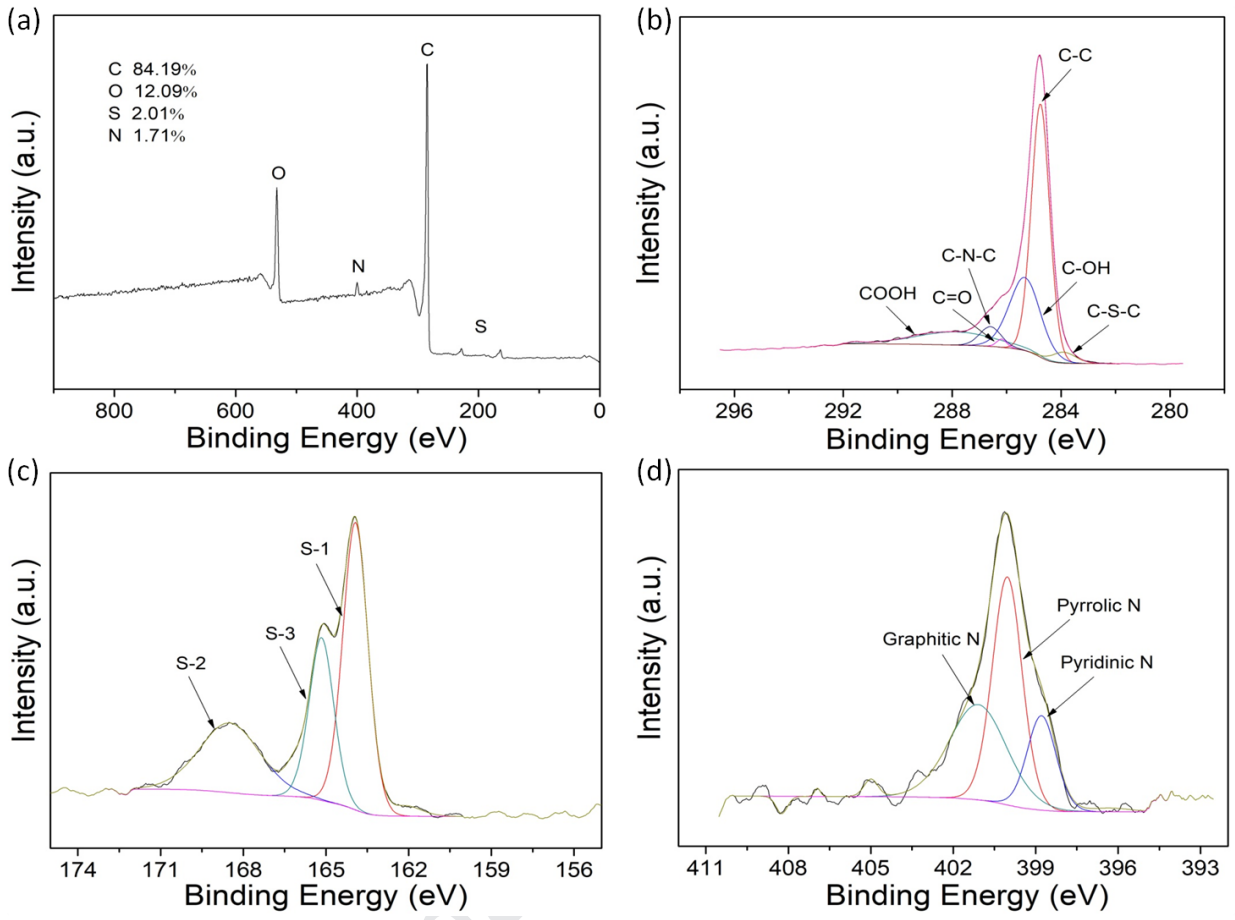
(a)
C 84.19%
O 12.09%
S 2.01%
N 1.71%
C
O
N
S
Intensity (a.u.)
800
600
400
200
0
Binding Energy (eV)
(b)
C-C
C-N-C
C-OH
COOH
C=O
C-S-C
Intensity (a.u.)
296
292
288
284
280
Binding Energy (eV)
(c)
S-1
S-3
S-2
Intensity (a.u.)
174
171
168
165
162
159
156
Binding Energy (eV)
(d)
Pyrrolic N
Graphitic N
Pyridinic N
Intensity (a.u.)
411
408
405
402
399
396
393
Binding Energy (eV)

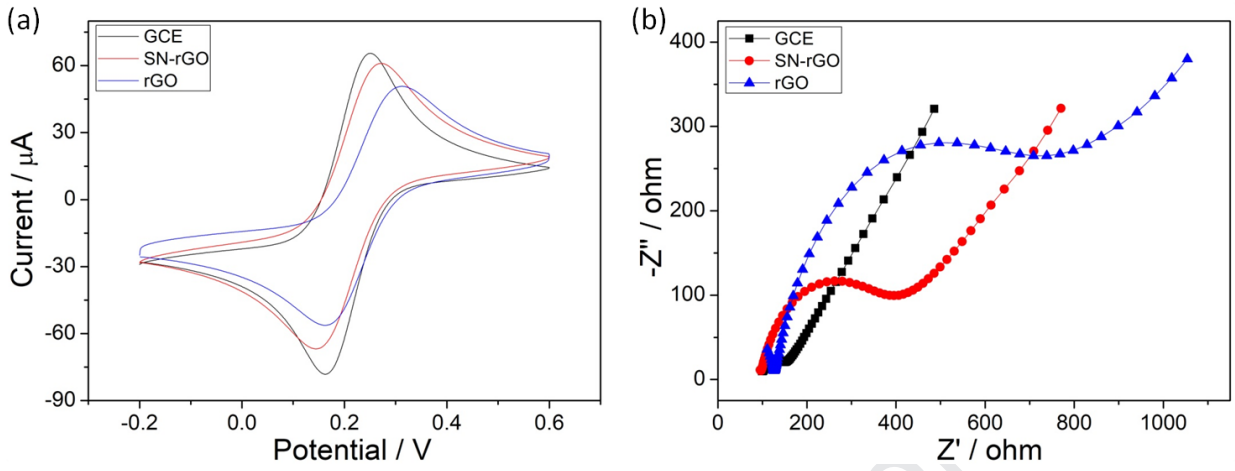

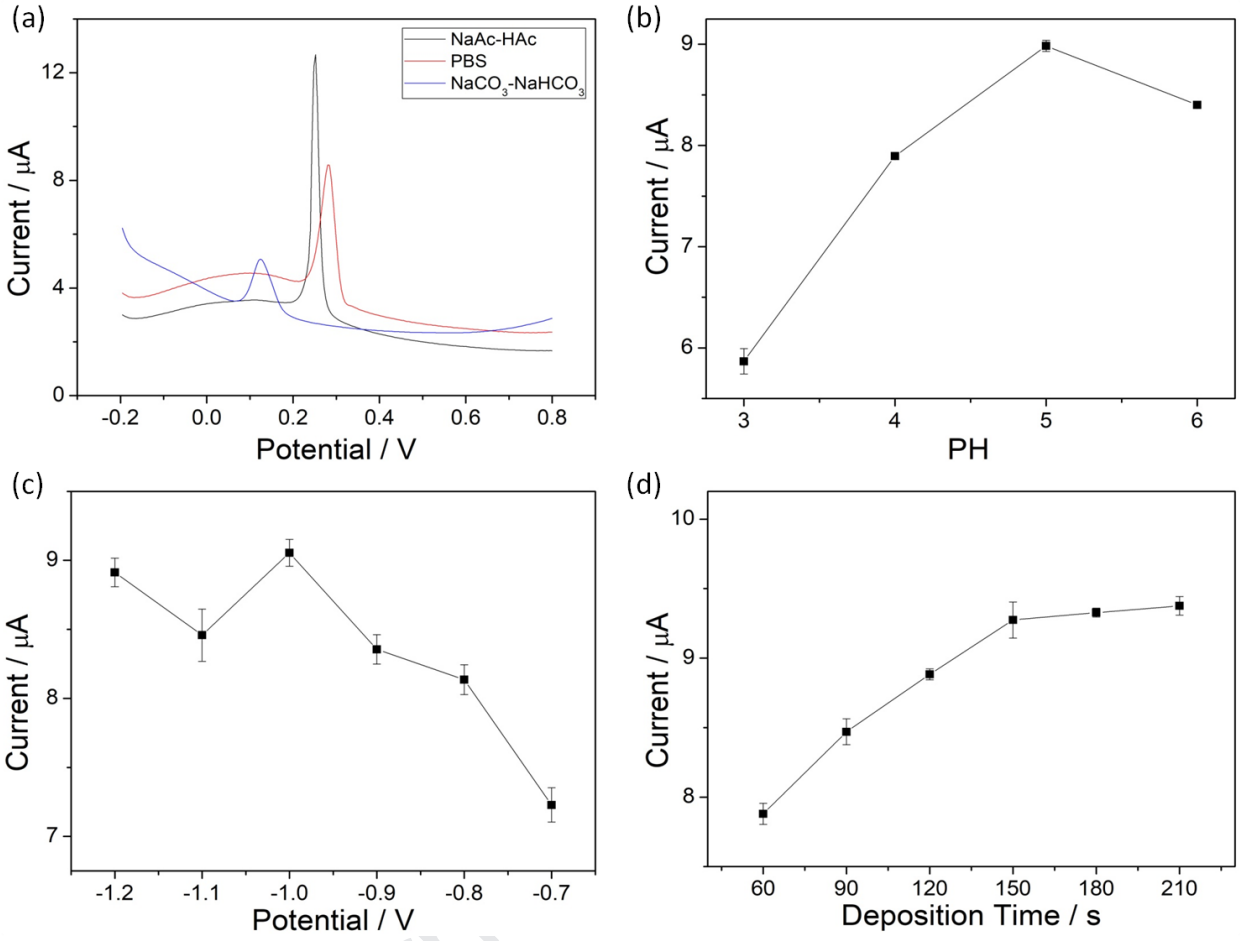
(a)
NaAc-HAc
PBS
NaCO3-NaHCO3
Current / μA
Potential / V
(b)
Current / μA
PH
(c)
Current / μA
Potential / V
(d)
Current / μA
Deposition Time / s

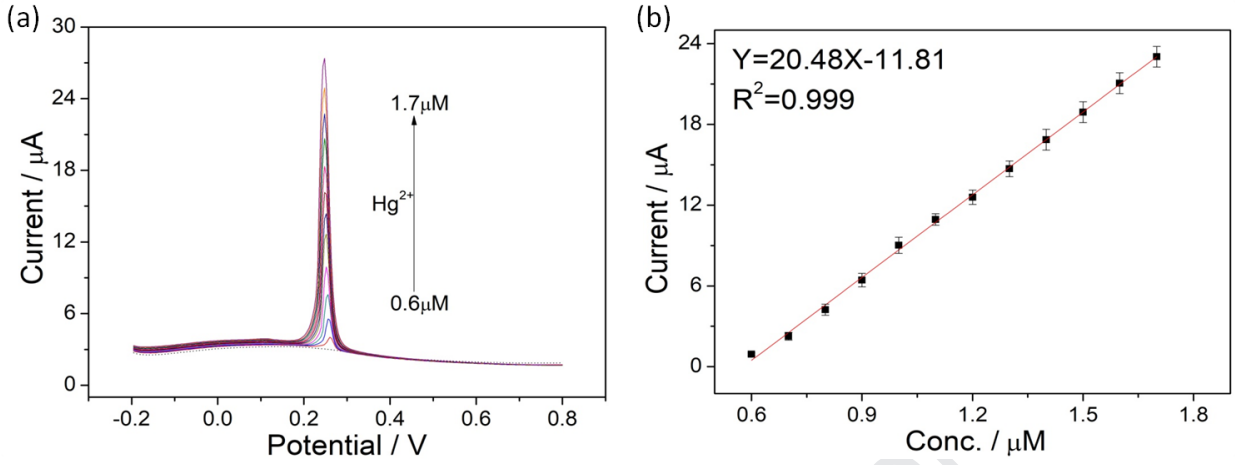

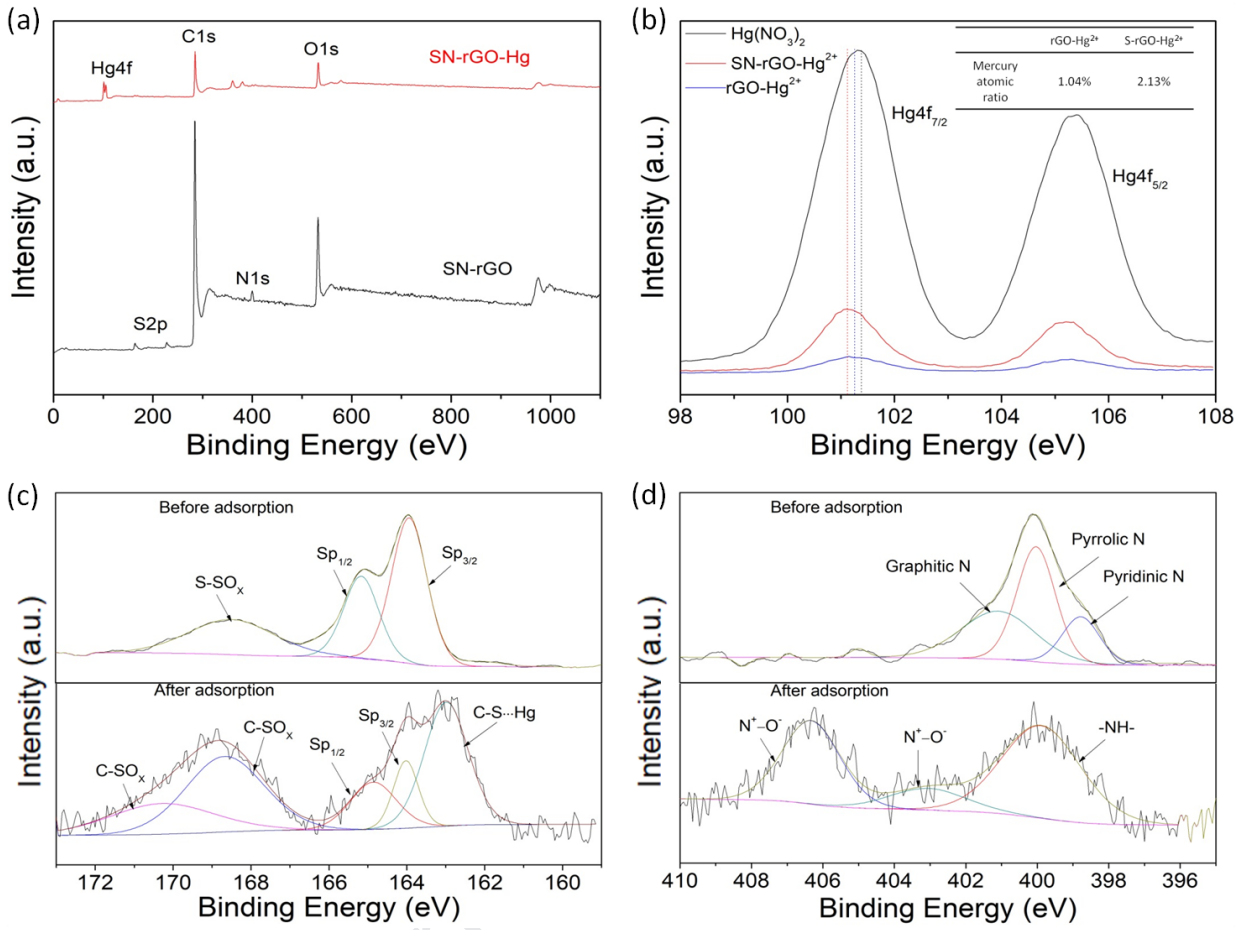
(a)
Hg4f
C1s
O1s
SN-rGO-Hg
N1s
SN-rGO
S2p
Intensity (a.u.)
Binding Energy (eV)
(b)
Hg(NO3)2
SN-rGO-Hg2+
rGO-Hg2+
rGO-Hg2+
S-rGO-Hg2+
Mercury atomic ratio
1.04%
2.13%
Hg4f7/2
Hg4f5/2
Intensity (a.u.)
Binding Energy (eV)
(c)
Before adsorption
S-SOx
Sp1/2
Sp3/2
After adsorption
C-SOx
C-SOx
Sp1/2
Sp3/2
C-S···Hg
Intensity (a.u.)
Binding Energy (eV)
(d)
Before adsorption
Graphitic N
Pyrrolic N
Pyridinic N
After adsorption
N+–O-
N+–O-
-NH-
Intensity (a.u.)
Binding Energy (eV)

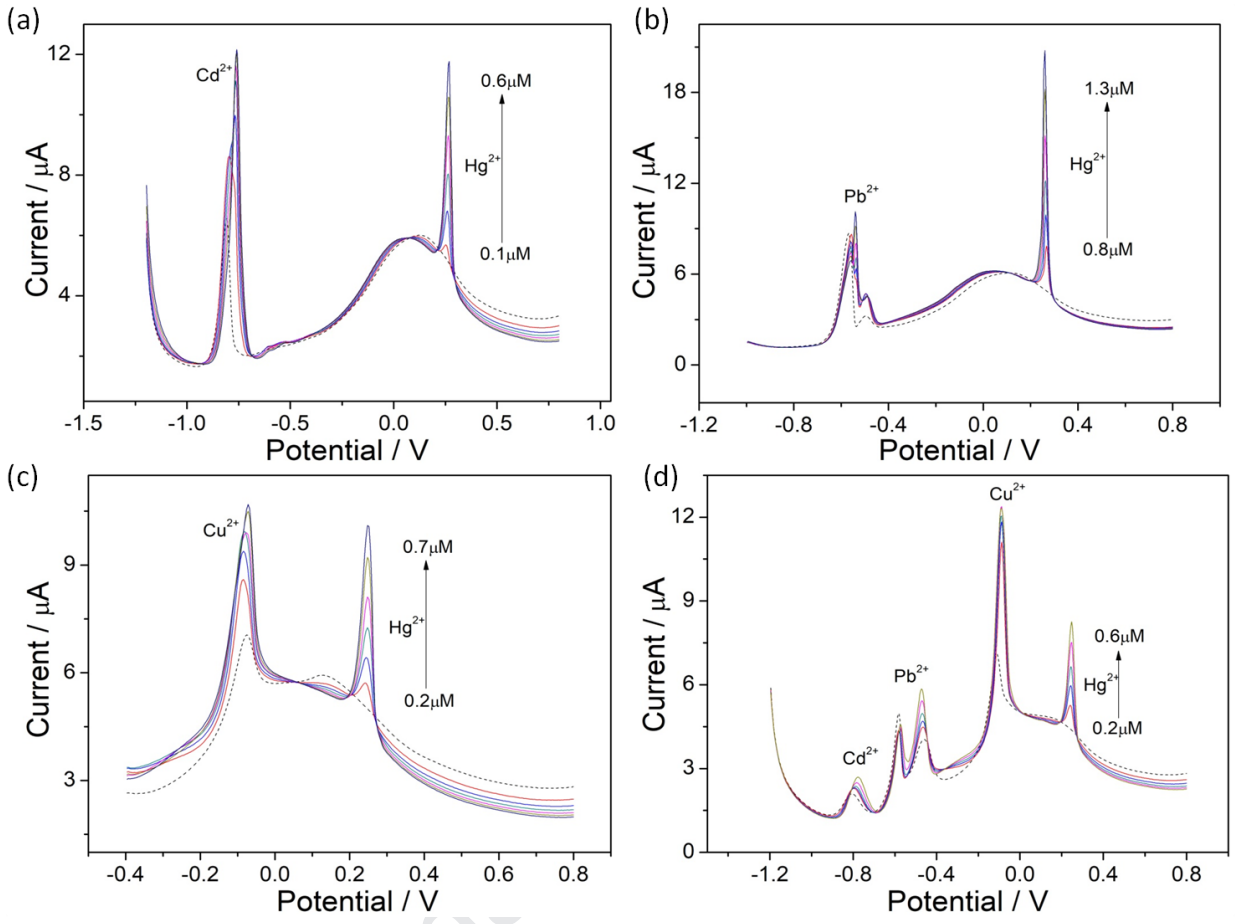
(a)
Cd2+
0.6μM
Hg2+
0.1μM
Current / μA
Potential / V
(b)
Pb2+
1.3μM
Hg2+
0.8μM
Current / μA
Potential / V
(c)
Cu2+
0.7μM
Hg2+
0.2μM
Current / μA
Potential / V
(d)
Cu2+
Pb2+
Cd2+
0.6μM
Hg2+
0.2μM
Current / μA
Potential / V

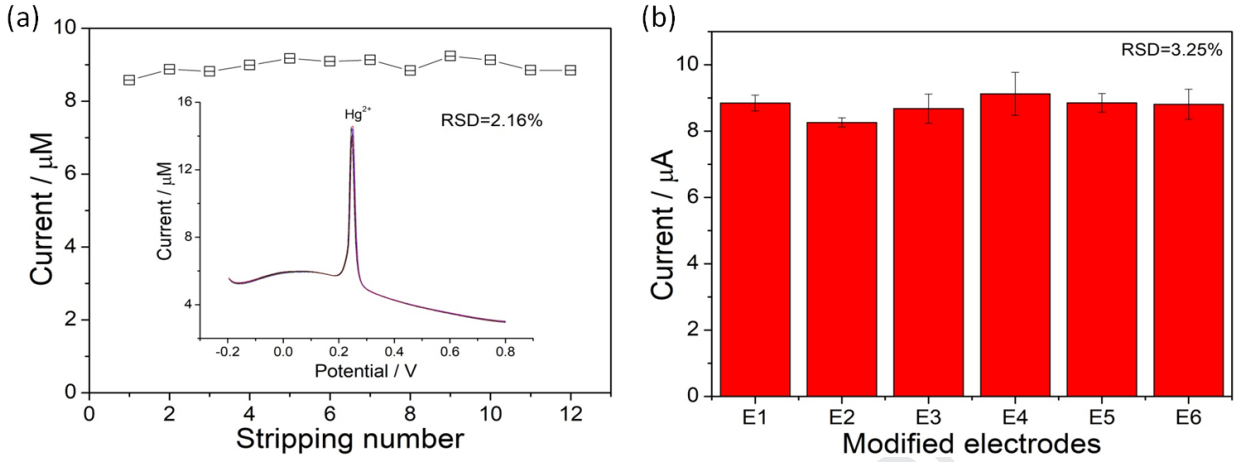

Highlights:

- S/N "hooks" were assembled on reduced GO(SN-rGO) via a one-step hydrothermal method
- SN-rGO modified GCE was used for electrochemical detection of Hg(II)
- Our sensor shows good sensitivity and anti-interference performance
- S/N groups enhance Hg(II) complexation for its electrochemical determination

Declaration of interests

☒ The authors declare that they have no known competing financial interests or personal relationships that could have appeared to influence the work reported in this paper.

☐The authors declare the following financial interests/personal relationships which may be considered as potential competing interests: